circEPSTI1 Enables Dengue Innate Immune Evasion by Sponging miR-942-5p, a Repressor of AKT1 and the Viral Genome

Nilanjana Das [a1], Pandikannan Krishnamoorthy [a1], Kushal Ramrao Junghare [a], Athira S Raj [a], Priyanka Saha [b], Kuhu Pal[b], Shouvanik Adhya [c], Atul Garg [d], Dheeraj Khetan [e], Ashok Kumar [f], Himanshu Kumar [a, g*]

Affiliations:

[a] Department of Biological Sciences, Laboratory of Immunology and Infectious Disease Biology, Indian Institute of Science Education and Research (IISER) Bhopal, Bhopal-462066, MP, India

[b] Department of Microbiology, College of Medicine and JNM Hospital, Kalyani, West Bengal.

[c] Department of Forensic Medicine and Toxicology, College of Medicine and JNM Hospital, Kalyani, West Bengal.

[d] Department of Microbiology, Sanjay Gandhi post graduate Institute of Medical sciences, Lucknow

[e] Department of Transfusion Medicine, Sanjay Gandhi Postgraduate Institute of Medical Sciences, Lucknow, India.

[f] Department of Biochemistry, All India Institute of Medical Sciences (AIIMS), Bhopal, Madhya Pradesh, India

[g] Laboratory of Host Defense, WPI Immunology, Frontier Research Centre, Osaka University, Osaka 5650871, Japan

1 These authors contributed equally.

***Corresponding author:** H Kumar, Department of Biological Sciences, Laboratory of Immunology and Infectious Disease Biology, Indian Institute of Science Education and Research

(IISER) Bhopal, AB-3, Room No. 220, Bhopal By-pass Road, Bhauri, Bhopal 462066, MP, India. Tel: +91 755 6691413; Fax: +91 755 669 2392; E-mail: hkumar@iiserb.ac.in

Running head: **circEPSTI1 regulates antiviral miR-942-5p during DENV infection**

ABSTRACT

Circular RNAs (circRNAs) are recently emerging transcripts that are gaining attention for their potential role in host-pathogen interactions. However, the role of circRNAs in Dengue virus (DENV) infection remains unexplored. In this study, circEPSTI1 induction was observed in DENV-infected peripheral blood mononuclear cells (PBMCs) and plasma of Dengue patients. circEPSTI1 induction is interferon-dependent, as IRF3-knockout cells completely abolished its induction. circEPSTI1 enhances DENV infection by sponging the expression of hsa-miR-942-5p. The antiviral role of hsa-miR-942-5p is mediated by bidirectional inhibition of conserved genomic sequences of the DENV genome across NS1, NS3 and NS5 and the host AKT1 signaling pathway. circEPSTI1 sponges hsa-miR-942-5p and relieves its inhibition over DENV genomic RNA and the host AKT1 signaling pathway, thus leading to increased AKT1 activation and DENV replication. These findings highlight the diagnostic and therapeutic potential of circEPSTI1 and the novel circEPSTI1-miR-942-5p-AKT1 axis that regulates the host immune response against DENV infection.

Keywords: circRNA; Dengue; Innate immunity; microRNA; Host-pathogen interaction

Introduction:

Dengue is an emerging global health threat due to the increased outbreaks and its distribution to over half of the global population (1). Dengue is linked to symptoms ranging from moderate fever in the case of Dengue fever (DF) to thrombocytopenia, vascular leakage in the case of Dengue with Warning signs (DWS), and excessive production of cytokines and organ dysfunction in the case of Severe Dengue (SD) (2). Different serotypes of the Dengue virus (DENV-1, DENV-2, DENV-3, and DENV-4) are transmitted through *Aedes* aegypti. The DENV genome is an 11kb positive-sense RNA genome consisting of a highly conserved 5'-UTR, a lengthy ORF coding polyprotein, and a very organized, unstable 3'-UTR. Secondary infection with a different serotype can lead to severe clinical outcomes through the process known as antibody-dependent enhancement, which limits the DENV vaccine development (3).

Host innate immunity plays a crucial antiviral role during DENV infection (4). DENV is sensed by Pathogen recognition receptors (PRRs) such as Toll-like receptors (TLR-3/7) and Retinoic-acid-like receptors (RLRs), which initiate type-I Interferons (IFN-α, IFN-β) production to limit DENV replication. RIG-I senses the DENV RNA and recruits a sole adaptor protein, IPS-1 (also known as MAVS, VISA, and CARDIF), subsequently activating transcription factor IFN regulatory factor 3 (IRF3) and NFκB to produce Type-I, Type-III IFN and inflammatory cytokines, respectively (5). However, DENV utilizes multiple strategies to evade the antiviral innate immunity and establish the infection, skew physiology, and develop a range of clinical symptoms (6).

Non-coding RNAs play an important role in regulating genes and various signaling pathways that are part of the antiviral immune responses (3). Non-coding RNAs can be categorized into small non-coding RNAs, such as microRNAs (length less than 200 nucleotides), and long non-coding RNAs, such as lncRNAs (length more than 200 nucleotides). An emerging class of transcripts, circRNAs, single-stranded, covalently-closed RNAs without free ends, formed through back-splicing, are shown to have higher diagnostic and therapeutic potential due to their excellent stability and presence in diverse cell types and extracellular fluids. CircRNAs were reported to regulate various biological processes in diseases like cancer, neurological disorders, and autoimmune diseases (7).

CircRNAs exert their mechanistic role by binding to RNA-binding proteins (RBPs) and are also well known to sponge microRNAs (miRNAs) (8). miRNAs are small non-coding RNAs that post-transcriptionally regulate the expression of genes by binding to the 3’-UTR of mRNAs. miRNAs can either bind to the mRNAs of the innate immune genes or bind to the viral genomes of RNA viruses and regulate the viral replication (9). The regulatory functions of miRNAs are further regulated by circRNAs and thus form a tight layer of competing endogenous RNA network to regulate various signaling pathways under different physiological conditions. The role of circRNAs in regulating innate antiviral immune response against viral infection is not well-studied. Most circRNA studies are related to DNA viruses, and no previous studies have explored the mechanistic role of circRNAs in DENV infection (10).

In this study, after the comprehensive computational analysis of the high-depth clinical RNA-seq dataset, circEPSTI1 was identified to be highly expressed and upregulated in the PBMCs of the

Dengue patients. The upregulation was validated in the plasma of Indian Dengue patients recruited for this study. Further, the characterization of circEPSTI1 revealed that the upregulation of circEPSTI1 is interferon-dependent, and the knockdown and overexpression of circEPSTI1 suppress and enhance the DENV replication, respectively. Mechanistically, circEPSTI1 exerts its pro-viral role by sponging hsa-miR-942-5p, a miRNA that suppresses DENV replication by targeting the DENV genomic RNA at NS1, NS3 and NS5 loci positions and host AKT1 signaling pathway. The sponging of hsa-miR-942-5p by circEPSTI1 relieves its suppression on AKT1, a key protein in cellular survival that DENV hijacks for replication, thus facilitating a conducive microenvironment for viral propagation. Thus, circEPSTI1 functions as a competing endogenous RNA (ceRNA) that modulates the host antiviral response by regulating the activity of miR-942-5p during DENV infection.

RESULTS:

Transcriptome-wide analysis of circRNAs dysregulation in Dengue-infected patients identifies circEPSTI1 upregulation:

The circRNAs are known to be dysregulated in the blood components upon different pathological conditions such as cancer and viral infections. However, the circRNAs dysregulated in Dengue patients compared to uninfected cases have not yet been identified. Quantifying circRNAs from RNA-seq datasets is possible from total-RNA libraries but not polyA-enriched libraries. Upon mining public transcriptome datasets for the DENV-infected clinical samples, only the dataset, GSE94892, was found to be derived from the total RNA library without polyA-enrichment (11). Identification of circRNAs was highly influenced by the depth of sequencing and the number of reads per sample. The sequencing depth was higher (more than 80 million reads per sample) and not poly-A enriched in this dataset. As illustrated in **(Fig. 1A)**, the distribution of mapped, unmapped, and circular reads supported accurate quantification of circular transcripts. Principal Component Analysis (PCA) revealed a clear segregation of Control and DENV-infected groups based on circRNA expression profiles **(Supplementary Fig. 1A)**, indicating distinct transcriptomic alterations during infection. Differential expression analysis identified 180 significantly dysregulated circRNAs (padj < 0.05, $|\log\square FC| > 1$), including 142 upregulated and 36 downregulated circRNAs, denoted by the volcano plot **(Fig. 1B)**. To identify clinically relevant circRNAs for translational application in clinical settings, it is important to find highly expressed circRNAs. The expression of the top circRNAs in each sample was visualized through the violin plot (**Supplementary Fig 1B**) and the heatmap **(Supplementary Fig**. **1C).** The dot plot **(Figure 1C)** representing the normalized counts of the top significant

circRNAs reveals hsa_circEPSTI1_001(circEPSTI1) with consistently higher expression across every sample (above the red dotted line denoting the normalized expression value of more than 5) and also significantly upregulated upon DENV-infected patients (triangle datapoints) compared to the control group (circle datapoints). circEPSTI1 (hsa_circ_0000479, in circBase) is derived by the back-splicing between the exon 2 and exon 6 of EPSTI1 pre-mRNA, leading to the 375 bp transcript (**Supplementary Fig. 2A)**. Circular RNAs are not expected to be amplified from genomic DNA (gDNA) as well as the cDNA synthesized through the oligo-dT method, as they lack poly-A ends. To ensure the circRNA is amplified but not the linear one, the divergent primer flanking the backsplice junction was designed to amplify the circEPSTI1, and the convergent primer was designed to amplify the linear ESPTI1 **(Fig. 1D)**. The genomic DNA and cDNA generated from human PBMCs through random hexamers were amplified with the divergent and convergent primers. circEPSTI1 was amplified only in the cDNA amplified through the random hexamer method but not gDNA and cDNA generated through the oligo-dT method. However, linear EPSTI1 was amplified in both the gDNA and cDNA from PBMCs **(Fig. 1D)**, suggesting the amplified product by divergent primer belongs to circEPSTI1 but not the linear counterpart. Similar results were obtained in the A549 cell line **(Supplementary Fig. 2 B).** Sanger sequencing of the amplified bands revealed the presence of the sequence of the back-splice junction of circEPSTI1 **(Fig. 1E)**. CircRNAs generally have higher stability than linear RNA. Actinomycin D (ActD) inhibits transcription by binding to DNA and inhibits the activity of RNA polymerase to synthesize new RNA, and hence can be utilized for measuring the stability of circRNA, compared to the linear RNA. Upon ActD treatment in PBMCs **(Fig.1F)** and A549 **(Supplementary Fig. 2C)**, linear EPSTI1 decreases, whereas circEPSTI1 remains stable, suggesting the amplified product is a circRNA. RNase R is a 3’-5’ exoribonuclease that can

selectively degrade linear RNAs but not circular RNAs. RNAse R treatment in PBMC **(Fig. 1G)** and A549 **(Supplementary Fig. 2D)** showed that the circEPSTI1 level remained unchanged, whereas linear EPSTI1 almost completely degraded. To gain insight of circEPSTI1 cellular localization, the nuclear and cytoplasmic fractions were isolated, and the level of enrichment of circEPSTI1 were measured. circEPSTI1 is predominantly distributed in the cytoplasm of the PBMCs **(Fig. 1H)** and A549 **(Supplementary Fig. 2E)**. To strengthen our biochemical observations, cell imaging was performed through Fluorescence in situ Hybridization (FISH) utilizing a Cy3-labelled probe targeting circEPSTI1. The enrichment in the cytoplasm of the A549 cells was observed as visualized through confocal microscopy **(Fig. 1I)**. Overall, computational analysis and multiple experiments suggested that the circEPSTI1 is one of the highly expressed circRNAs in DENV-infected patients and possesses the properties of the circRNAs and is widely distributed in the cytoplasm.

DENV infection upregulates circEPSTI1, and induction is interferon-dependent

To validate the prediction from the RNA-seq results, clinical recruitment of DENV patients was performed. RNA from the plasma of healthy controls and Dengue patients was isolated, and the level of circEPSTI1 was measured by qPCR. circEPSTI1 level was found to be upregulated significantly in the DENV patients compared to the healthy controls **(Fig. 2A)**.

PBMCs from the healthy volunteers were isolated and infected with DENV ex vivo, and circEPSTI1 level was found to be upregulated **(Fig. 2B)**, as observed in the plasma. Next, the copy number of circRNA in A549 cell was determined because it is crucial for therapeutic manipulation. To this end a highly sensitive, digital-PCR method was utilized to measure the

copy number of circEPSTI1, and it is observed that the copy number of circEPSTI1 is very low in uninfected cells, and upon infection, it increases to 750 copies (more than 7 times) per ul **(Fig. 2C)**. This suggests that the expression and copy number of circEPSTI1 are increased upon DENV infection. Further, to understand the dynamics of the induction of circEPSTI1, different cell lines were infected with DENV, and the circEPSTI1 level was measured post 12, 24, 36, and 48 hours of infection. circEPSTI1 levels were not upregulated till 12 hours post-infection, and subsequently, the expression was increased in PBMCs, A549, MRC5, and HEPG2 cell lines **(Fig. 2D)**. Overall, circEPSTI1 induction upon DENV infection was observed in diverse cell types, and the magnitude and extent of expression vary between different cell types and DENV infectivity (**Supplementary Fig. 3)**. Upon DENV infection, the primary innate antiviral response is initiated by TLR-3 signaling and RLR signaling that induces type-I interferons and inflammatory cytokines. Upon TLR-3 ligand, Poly(I:C) stimulation, circEPSTI1 was induced as observed in the case of viral infection **(Fig. 2E)**, and treatment of cells with type-I interferons, IFN-α and IFN-β, also induced circEPSTI1 expression, suggesting the role of interferon-mediated induction, rather than DENV-specific induction **(Fig.2F, 2G)**. To explore the involvement of type-I interferon signaling for circEPSTI1 induction and whether it is RLR-dependent, the innate immune RLR sensor, RIG-I, RLR signaling adaptor IPS-1 (also known as MAVS, VISA, CARDIF), and the downstream interferon-inducing transcription factor, IRF3, were knocked out using the CRISPR-Cas9 technique in A549 cells. DENV infection was performed in the WT, RIG-I KO, IPS-1 KO, and IRF3 KO cells at different time points. circEPSTI1 was induced in WT cells but not induced in the cells deficient in RIG-I, IPS-1, and IRF3, suggesting the interferon-dependent induction of circEPSTI1 **(Fig. 2H)**. In the previous section, cellular localization of circEPSTI1 was shown to be predominantly present in the

cytoplasm. Therefore, cellular localization of circEPSTI1 was imaged upon DENV infection by confocal microscopy as described previously. The results revealed the significant enrichment of circEPSTI1 in the cytoplasm of DENV-infected cells **(Fig. 2I)**. Taken together, circEPSTI1 induction upon DENV infection is observed to be interferon-dependent and is predominantly expressed in the cytosolic compartment.

circEPSTI1 regulates DENV infection

The effect of induction of circEPSTI1 over DENV replication was explored by the siRNA-mediated knockdown study. siRNA was designed to target the back-splice junction of circEPSTI1, and the knockdown of circEPSTI1 was verified by RT-PCR in both human PBMC and A549 cells, as shown in **Fig. 3A**. The siRNA reduced 45% to 60% expression in these cells. Knockdown of circEPSTI1 led to a reduction in the viral load in both PBMC and A549 cells and culture supernatant **(Fig. 3B & C)**. Similar effects were observed in THP1 and MRC5 cell lines (**Supplementary Fig. 4A and 4B**). To further investigate the effect of circEPSTI1 knockdown on DENV viral load, western blot, Flow cytometry, and confocal microscopy were performed using DENV NS5-specific antibodies. At the protein level, the dengue NS5 level was suppressed upon knockdown of circEPSTI1 **(Fig. 3D)**. Flow cytometry analysis revealed a reduction of DENV in the circEPSTI1 knockdown **(Fig.3E)**, and confocal microscopy also showed a reduction in the intensity of DENV in circEPSTI1 knockdown cells **(Fig. 3F)**. Collectively, our results with multiple techniques demonstrate that circEPSTI1 knockdown was found to suppress DENV replication. To strengthen the findings, circEPSTI1 overexpression was performed by cloning circEPSTI1 in the mc2mNeonV2 vector, and the overexpression was verified by RT-

PCR, which shows a more than 1400-fold increase in circEPSTI1 **(Fig. 3G)**. DENV viral load was increased to a higher extent upon circEPSTI1 overexpression in A549 cells and in culture supernatant **(Fig. 3H & I).** The finding was further validated through western blot **(Fig. 3J)**, flow cytometry **(Fig. 3K)**, and confocal microscopy **(Fig. 3L)**. Altogether, the DENV viral load increased upon circEPSTI1 overexpression, as demonstrated by various assays. Next, the innate antiviral responses were measured, interferon-induced genes, such as IFN-β and OAS2, were significantly increased and suppressed upon knockdown **(Fig. 3M)** and overexpression **(Fig. 3N)** of circEPSTI1, respectively. The levels of IFN-inducible protein, IP-10 and inflammatory cytokine IL-6, in culture supernatant upon circEPSTI1 knockdown, were significantly enhanced **(Fig. 3O)**. Similarly, IP-10 and IL-6, in culture supernatant upon circEPSTI1 overexpression, were significantly reduced **(Fig. 3P)**. Overall, knockdown of circEPSTI1 reduces the viral load and increases IFNβ and inflammatory cytokines, whereas overexpression of circEPSTI1 increases the viral load and decreases the level of IFNβ and inflammatory cytokines, suggesting the pro-viral role of circEPSTI1 facilitating DENV replication.

circEPSTI1 sponges miR-942-5p during DENV infection

Circular RNAs exert their regulatory functions mainly by sponging miRNAs and stabilizing the target transcripts, which subsequently result in sustained protein expression. The miRNAs binding to circEPSTI1 are predicted by three widely utilized algorithms- miRanda, PITA, and TargetScan. miRanda predicts the sequence complementarity between the circRNA and miRNA and the thermodynamic stability of the interaction, and calculates the binding energy and score. hsa-miR-942-5p was the top miRNA with the lowest free energy and the highest miRanda score.

PITA considers the accessibility and miRNA-target pair and computes free energy, and Target Scan considers seed region complementarity, conservation, and number of sites. miR-942-5p was the common miRNA predicted by all three tools with a stringent cutoff **(Fig. 4A)**. To validate the predictions, the circRNA sequence was cloned downstream of luciferase under the CMV promoter as shown in schematic of **Fig. 4B**. Upon overexpression of hsa-miR-942-5p, the luciferase activity of the circEPSTI1-luc vector was reduced significantly, indicating that hsa-miR-942-5p binds to circEPSTI1 and suppresses its expression. In contrast, when the hsa-miR-942 inhibitor was introduced which sequester endogenous hsa-miR-942-5p, the luciferase activity was not reduced, suggesting the suppression is not due to non-specific binding **(Fig. 4B)**. To further validate the finding, the predicted binding sites of miR-942 in the circ-EPSTI1 sequence were mutated, and this mutated construct failed to reduce the luciferase activity upon hsa-miR-942 overexpression, suggesting that miR-942 binds to circEPST1 with its seed sequence at the predicted sites **(Fig. 4C)**. The miRNA targets the transcript through a multiprotein complex known as RNA-induced silencing complex (RISC) and Argounate-2 protein (AGO2) is one of essential component of RISC for miRNA-mediated silencing. To explore the involvement of AGO2 in circEPSTI1 and hsa-miR-942-5p interaction, the AGO2 pulldown assay was performed using a FLAG-specific antibody. The cells transfected with hsa-miR-942 showed greater than four fold enhancement of circEPSTI1 levels in the pull-down fraction compared to the NC-transfected cells **(Fig. 4D)**. Conversely, to further validate the findings, circEPSTI1 was pulled down using biotin probes and hsa-miR-942-5p levels were enriched in the pull-down fraction in circEPSTI1 overexpressed cells compared to the control vector transfected cells, suggesting circEPSTI1 and hsa-miR-942-5p bind with each other **(Fig. 4E)**. To assess the functional consequences of this interaction, upon knockdown of circEPSTI1,

hsa-miR-942-5p levels were quantified. hsa-miR-942-5p levels were significantly upregulated upon circEPSTI1 knockdown in PBMCs and A549 cells compared to the negative control transfected cells **(Fig. 4F)** suggesting the inverse regulatory relationship between circEPSTI1 and hsa-miR-942-5p. Interestingly, simultaneous siRNA-mediated knockdown of circEPSTI1 and inhibition of hsa-miR-942-5p through the inhibitor restored the DENV viral load achieved only by knocking down circEPSTI1. **(Fig. 4G)**. This implies that the pro-viral activity of circEPSTI1 is mediated through the regulation of hsa-miR-942-5p expression. Further, miR-942-5p expression was suppressed upon DENV infection at different time points in PBMC, A549, MRC5, and HEPG2 cell lines, negatively correlated with the induction of circEPSTI1 expression. **(Fig. 4H).**

hsa-miR-942-5p targets the DENV genome and inhibits DENV replication

MicroRNAs bind to the genome of RNA viruses such as Influenza and regulate their replication (9, 12). The miRanda tool was utilized to find whether miR-942-5p can bind to the DENV genomic RNA across all four serotypes **(Fig. 5A)**. Based on the conservation of the site across more than one DENV serotype and the free energy, 8 sites in the DENV genome were identified. NS5 bears 4 sites, NS1 bears 3 sites, NS3 bears 2 sites, and E bears a single site **(Supplementary Fig. 5A)**. To validate the prediction, NS5, NS3, and NS1 were cloned downstream to the luciferase, and the luciferase activity upon miR-942-5p overexpression was measured. NS1 luciferase activity was suppressed the most, followed by NS3 and NS5. When NS2B with no predicted binding site was cloned downstream of luciferase, luciferase activity suppression was not observed, suggesting the predictions are not random and non-specific **(Fig. 5B)**. To determine the involvement of AGO2-mediated miR-942-5p DENV viral RNA

interaction, AGO2 pulldown was performed and DENV RNA was enriched in the pull-down fraction compared to the control uninfected cells **(Fig. 5C)**. miR-942-5p overexpression in A549 and PBMC also reduced the DENV levels significantly. The same effect was not observed when the miR-942-5p inhibitor was used **(Fig. 5D).** The suppression of DENV load was also observed in the supernatant in A549 cells **(Fig. 5E)**. The level of NS1 and NS5 at the protein level was evaluated through the western blot. DENV protein levels were reduced upon miR-942-5p overexpression, suggesting the anti-viral role of miR-942-5p upon DENV infection **(Fig. 5F)**. Further, the reduction of DENV NS1 and NS5 was validated by FACS **(Fig. 5G)** and Immunofluorescence through confocal microscopy **(Fig. 5H)** using NS1 and NS5-specific antibodies. Further, the levels of interferon-inducible protein, IP-10 and inflammation-associated cytokines such as IL-6 was measured through ELISA, and it was observed that upon miR-942-5p overexpression, IL-6 and IP-10 levels were significantly induced **(Fig. 5I)**. Overall, miR-942-5p suppresses DENV infection by primarily targeting the DENV NS1 and NS5 and to some extent NS3 to modulate the host innate immune response.

miR-942-5p targets the host Akt-signaling pathway and regulates DENV infection:

To identify the host targets of miR-942-5p, miRabel tool was utilized, which reports the top host genes based on different miRNA-binding tools (13). Upon performing the pathway enrichment analysis of miR-942-5p targets, we found AKT1 signaling pathway as one of the enriched pathways, next to metabolic and cancer pathways **(Fig. 6A)**. Furthermore, NS1, NS3, and NS5 were found to interact with various proteins involved in PI3K/AKT signaling (**Supplementary Fig. 5B**). Various factors activate AKT1 signaling, and the phosphorylation of AKT1 (S473)

indicates one of the activation mechanisms of the pathway (14). The level of p-AKT1 (S473) decreases in initial time points and increases until 48 hours post-DENV infection **(Fig. 6B)**, suggesting the activation of the AKT1 signaling pathway upon DENV infection. Among the target genes predicted to be bound by miR-942-5p, AKT1 was the central mediator of this pathway. The 3'UTR of AKT1 was cloned downstream to luciferase, and the luciferase activity was suppressed when miR-942-5p was overexpressed in HEK293T cells. However, miR-942-5p inhibitor did not suppress the luciferase activity **(Fig. 6C)**. Further mutation of the miR-942-5p binding site in AKT1 UTR could not reduce the luciferase activity, proving the specific interaction of miR-942-5p with the 3'-UTR of miR-942-5p **(Fig. 6D)**. AGO2-pulldown upon miR-942-5p showed enrichment of AKT1 level. The enrichment was not observed when the miR-942-5p inhibitor was used **(Fig. 6E)**. At the protein level, AKT1 was suppressed upon miR-942-5p overexpression during DENV infection **(Fig. 6F).** Overall, miR-942-5p was found to target viral genomic RNA as well as the host AKT1 RNA and modulate the AKT1 signaling pathway. To know the role of AKT1 in DENV infection, siRNA-mediated knockdown of AKT1 was performed. The knockdown of AKT1 reduced the DENV viral load, suggesting the pro-viral role of AKT1 **(Fig. 6G)**. At the protein level, the reduction in the protein level of NS5 was observed upon AKT1 knockdown **(Fig. 6H)**. The reduction in viral load upon siAKT1 knockdown was further validated by FACS **(Fig. 6I)** and confocal microscopy **(Fig. 6J)**. IFN-β and interferon-induced gene OAS2, were significantly increased upon siAKT1 knockdown **(Fig. 6K)**. The levels of interferon induced gene IP-10 and inflammatory cytokine IL-6 were quantified through ELISA and were found to be induced significantly upon AKT1 knockdown (**Fig. 6L)**. To know the role of circEPSTI1 in miR-942-5p-mediated AKT1 reduction, sicircEPSTI1 was transfected at increasing concentrations, and it was observed that AKT1 at the

protein level was decreased upon the increased dose of sicircEPSTI1. Upon DENV infection, when the siRNA-mediated suppression of circEPSTI1 was performed, its sponging activity on miR-942-5p was reduced, leading to more availability of miR-942-5p and hence leading to higher AKT1 suppression **(Fig. 6M)**. Overall, circEPSTI1 regulation of antiviral miR-942-5p that interacts with both viral RNA and host AKT1 can be the immune evasion strategy of DENV, utilizing the AKT1 signaling pathway. The pharmacological inhibition of AKT1 signaling was performed by Wortmannin treatment at two different doses. The reduction in viral load upon Wortmannin treatment was confirmed by Western blot analysis **(Fig. 6N)** and confocal microscopy **(Fig. 6O)**, suggesting a promising target molecule to target this axis and a promising DENV therapeutic target.

Discussion

CircRNAs have recently gained attention due to their diagnostic and therapeutic potential across different pathological conditions (8). In recent years, thousands of circRNAs have been identified and characterized across several tissues and many diseases (7). The role of circRNAs in regulating immune responses against the virus infection has not been well studied. circRNAs play an important role in the regulation of the miRNAs that, in turn, can regulate the genes, subsequently cellular signaling pathways, and finally disease outcome (7). The regulation by non-coding RNAs impacts cell signaling and shapes the complex host-pathogen interactions and the disease pathology (3). CircRNA detection methods from the high-throughput RNA-sequencing methods demand non-polyA enriched libraries and higher read depth to detect a significant number of circRNAs. Upon DENV infection, the role of the circRNAs has not been previously studied. Using microarray, two circRNAs were identified to be dysregulated between pretreatment and post-treatment whole blood samples of non-severe dengue patients (15). This study also did not explore the functional role of the identified circRNAs (15).

In this study, using computational analysis of RNA-sequencing datasets, circEPSTI1 was found to be significantly upregulated in the PBMCs of dengue patients compared to the control group and also bears higher expression in the blood (**Fig. 1C**). To validate the findings, the dengue patients were recruited from India, and using RT-PCR, the circEPSTI1 was found to be upregulated in the plasma of severe and non-severe dengue patients compared to the healthy controls, revealing its diagnostic potential (**Fig. 2A**).

circEPSTI1 was reported to be upregulated in several cancers, including cervical cancer (16, 17), osteosarcoma (18), breast cancer (19), non-small cell lung cancer (20, 21), ovarian cancer (22), and oral cancer (23). Increased expression of circEPSTI1 was reported to correlate with increased cell proliferation, migration, invasion, and overall tumor progression (16, 17, 20). Combination of circEPSTI1 and MIF (Macrophage Migration Inhibitory Factor) was reported to have diagnostic value in endometrial cancer (24). Apart from cancer, circEPSTI1 was also found to be a potential biomarker candidate in SLE (25). However, the expression of circEPSTI1 in virus infections and its role have not been previously studied. Hence, this study aimed to explore the functional role of circEPSTI1 in regulating the host immune response during DENV infection.

Host pathogen recognition receptor (PRRs) plays an important role in recognizing the viral elements to initiate host innate immune responses (26). Upon DENV infection, TLRs such as TLR3 (27) and TLR7 (28), RLRs such as RIG-I (29), were reported to recognize DENV RNA and initiate downstream interferon signaling. circEPSTI1 levels were upregulated upon PolyIC stimulation (a TLR3 Ligand), and recombinant IFN-α and β treatment. Interestingly, circEPSTI1 induction upon DENV infection was not observed in RLR sensor, RIG-I, RLR signaling adaptor, IPS-1, and the transcription factor IRF-3 knockout, suggesting interferon-dependent induction (**Fig. 2H**). Further functional analysis of circEPSTI1 by siRNA-mediated knockdown and overexpression revealed its pro-viral role in DENV replication **(Fig. 3)**.

Circular RNAs were reported to exert their function by binding to RNA-binding proteins (RBPs) and acting as a sponge for miRNAs (3, 8). To further elucidate the mechanism by which circEPSTI1 regulates DENV infection, the miRNA sponging activity of circEPSTI1 was explored. Through three different algorithms, the top host miRNA predicted to be targeted by

circEPSTI1 was found to be hsa-miR-942-5p. The cytoplasmic localization of circEPSTI1 further supports its functional relevance in regulating miRNA and protein interactions during DENV infection (**Fig. 2I**). Since circRNAs are known to interact with RNA-binding proteins (RBPs) and components of the RNA interference machinery, the cytoplasmic presence of circEPSTI1 may facilitate efficient sequestration of miR-942-5p, thereby modulating the downstream immune and signaling responses. This prediction is validated using the luciferase assay and AGO2-pull-down experiments (**Fig. 4**). hsa-miR-942-5p has been previously reported to play a role in antiviral responses and immune regulation upon HCV infection (30). However, its role in DENV infection has not yet been explored. The level of hsa-miR-942-5p was suppressed upon DENV infection (**Fig.4I**).

miRNAs exert their functions by binding to the 3'-UTR of the genes and to the viral genome of RNA viruses and regulating the host immune responses (9, 12). To explore whether hsa-miR-942-5p can bind to the DENV genome, the genomic sequences of all four serotypes of DENV were scanned for the presence of miR-942-5p binding sites. A total of 8 binding sites were identified and conserved in more than two serotypes (**Fig. 5A**). Out of which, NS5, NS3, and NS1 bear more sites. Prediction was further validated using luciferase assay and AGO2-pulldown experiments. hsa-miR-942-5p overexpression reduced DENV replication by binding to DENV NS5, NS3, and NS1. However, the host genes and the pathways that interplay with this interaction were unclear.

To identify the host hsa-miR-942-5p targets, the miRabel tool that reports the top gene candidates based on the results of multiple algorithms was utilized. The enrichment analysis of the top hits identified the genes belonging to broader cancer and metabolic pathways, followed by the specific AKT1 signaling pathway (**Fig. 6A**). DENV proteins were reported to interact

with the host AKT1 signaling proteins and modulate the pathway at the protein level (31). The suppression of miR-942-5p upon DENV infection, mediated by circEPSTI1, likely results in the dysregulation of downstream signaling pathways that promote viral replication. Specifically, circEPSTI1-mediated miR-942-5p sponging was linked to the activation of the AKT1 signaling pathway, which has been implicated in supporting viral replication and immune evasion. This highlights a novel mechanism by which DENV manipulates host cellular signaling through circRNA-mediated miRNA regulation.

Among the AKT1 signaling-related targets, the effector protein AKT1 was predicted to be targeted by hsa-miR-942-5p and validated using functional experiments. AKT1 is a serine/threonine kinase that plays a crucial role in cell survival, metabolism, and innate immune regulation. The AKT1 signaling activation is mediated through the phosphorylation of AKT1 at Serine 473 residue (p-AKT1). Multiple viruses utilize this pathway to promote their replication (14, 32). However, the interplay of AKT1 signaling and virus immunity is complex and was reported to be proviral as well as antiviral in different virus infections. A previous study reported the pro-viral role of AKT1 signaling upon DENV infection (33).

In this study, upon DENV infection, p-AKT1 level was increased, indicating the activation of AKT1 signaling. Both siRNA-mediated knockdown and pharmacological inhibition by wortmannin increase the DENV replication. Overexpression of hsa-miR-942-5p and siRNA-mediated knockdown of circEPSTI1 reduced the AKT1 level, suggesting the novel regulatory axis of circEPSTI1-hsa-miR-942-5p-AKT1 that modulates the host-virus interactions.

CONCLUSION

circEPSTI1, found to be upregulated in the plasma of Dengue patients, the correlation of circEPSTI1 level with the different severity is not yet known. Although circEPSTI1 is conserved, the divergent primers designed at the back-splice junction of the circEPSTI1 could not amplify the desired sequence in the mouse macrophages. Future studies are needed to explore the correlation between circEPSTI1 levels and the dengue severity and the mechanistic role in in-vivo models. Since DENV naturally doesn't infect mice, adapted mouse models susceptible to DENV infection can be utilized to explore the mechanistic role of circEPSTI1 upon DENV infection in vivo. Despite these shortcomings, to our knowledge, this is the first study that explored the role of any circRNA upon DENV infection and also shows a high potential for the clinical diagnosis of Dengue. Further research focusing on the clinical validation of circEPSTI1-based diagnostics and the development of therapeutic strategies targeting circEPSTI1 could provide new avenues for the management and treatment of dengue.

Materials and Methods

Reanalysis of publicly available data from the NCBI-GEO database

Publicly available RNA-sequencing datasets related to Dengue virus infection clinical samples in which Total RNA-sequencing was performed were retrieved from the NCBI-GEO database. Only one dataset (GSE94892) was found eligible for the study(11, 34). The raw sequencing reads were downloaded and quality-checked. Adapter trimming and low-quality read filtering were performed using fastp (35). The clean reads were aligned to the human reference genome (GRCh38) using the BWA aligner (36). The unmapped reads were further processed for circRNA detection using the CIRI2 algorithm (37). The quantification of circRNAs was performed through CIRIquant (38). The circRNA expression counts were pre-filtered with rowsums more than 5 in at least 10 samples to avoid the least-expressing circRNAs with zero counts. Differential expression analysis between DENV-infected and control samples was performed using DESeq2 (39). The top differently expressed circRNAs (DEcircRNAs) were identified based on the adjusted p-value and the logFC. The top DECircRNAs were visualized through a heatmap, a violin plot, and a dot plot using the ggplot2 R package.

Cells and transfection

A549 human alveolar basal epithelial cells (ATCC CCL-185), HEK293T human embryonic kidney cells (ATCC CRL-3216), HepG2 human hepatoblastoma cell line (HB-8065) and MRC5 Medical Research Council cell strain 5 (ATCC CCL-171) were grown in Dulbecco's modified Eagle's medium (DMEM) supplemented with 10% fetal bovine serum (FBS) and 1% penicillin-streptomycin. DNA, siRNA, or poly I:C transfection was carried out using Lipofectamine 3000 (Invitrogen). For electroporation of human PBMCs 1 × 10^6 cells were resuspended in Opti-

MEM (Invitrogen) containing 50 nM miRNA mimics (ThermoFisher Scientific). The cells were subjected to two pulses of 1000 V for 0.5 ms with a 5-second interval between pulses using the Gene Pulser Xcell electroporation system. Following electroporation, the cells were transferred to RPMI supplemented with 10% FBS.

Generation of the DENV-2 virus

Dengue virus (strain DENV-2, New Guinea C) virus was used in this study. Dengue virus was rescued from the reverse genetic system gifted by Prof. Andrew D Davidson, University of Bristol (40). Briefly, the plasmid was cloned into a low-copy-number plasmid pWSK29. Transformation of the vector pWSK29 was done into E. coli (DH5α) followed by overnight incubation and plasmid DNA isolation. Xba I linearized pDVWS601 plasmid was transcribed in vitro using a T7 RNA transcription kit followed by determination of the concentration of the RNA. For virus recovery, BHK-21 cells were transfected using DENV-2 transcripts, and the virus was harvested 48 hours after transfection. The cells were fixed, over-dried, and then assayed for evidence of viral replication by immunofluorescence assay using an antibody recognizing the DENV E protein. The remaining supernatant was used for the setup of passage 1 on C6/36 cells and for RT-PCR analysis.

Viruses and infection

Cells were washed with PBS and infected with 0.5 MOI DENV-2 virus dissolved in SF-DMEM. After 1.5 hrs, cells were washed with PBS again and incubated with SF-DMEM supplemented with 1% FBS.

PBMC isolation

Human PBMCs were collected from healthy donors using EDTA blood tubes and isolated using Histopaque-1077 (Sigma) as per manufacturer's guidelines. The cells were cultured in RPMI 1640 media supplemented with 5% FBS. The cells were infected with MOI=1.

Quantitative real-time reverse transcription-PCR

Intracellular RNA was extracted using TRIzol reagent (Invitrogen) while RNA from supernatant and patient samples were isolated by TRIzol LS reagent (Invitrogen) and then converted into cDNA with the High-Capacity cDNA synthesis kit (ThermoFisher Scientific) as per the manufacturer's guidelines. Gene expression was evaluated through quantitative real-time PCR using gene-specific primers and PowerUp SYBR Green Master Mix (ThermoFisher Scientific).

RNA Fluorescence in situ hybridization

A549 cells were seeded in 24-well plate and infected with DENV virus at an MOI=0.5 for 36h. The cells were fixed with 4% formaldehyde for 20min and permeabilized with 0.1% Triton X-100 for 5 min. The cells were treated with prehybridization buffer (2X saline sodium citrate buffer, 10% formamide) for 20min at room temperature. The cells were then hybridized in hybridization buffer (10% Dextran sulfate, 4X SSC, 40% formamide, 10×10^{-3} M DDT, 100 µg/ml yeast tRNA, 100 µg/ml sheared salmon sperm DNA, 1X Denhardt's solution) with 2 µl of Cy3-labeled circEPSTI1 probe at 55°C overnight. The cells were washed with PBS and the nuclei was stained with DAPI. The images were taken with LSM 780 confocal laser microscope.

Digital PCR

RNA was extracted with Trizol and cDNA synthesis was done using High-Capacity cDNA synthesis kit (ThermoFisher Scientific) as per the manufacturer's guidelines. dPCR reactions were performed using A549 cell line as template and circEPSTI1 primer using the kit QIAcuity EG PCR Kit (250111, QIAGEN).

Luciferase reporter assay

HEK 293T cells were seeded in 24-well plates and transfected at 60–70% confluency with 30 ng of the control plasmid pRL-TK, 100 ng of the luciferase reporter plasmid, and 25 nM of the control or miR-942 mimic. Cells were collected and lysed 36 hours post transfection, and luciferase activity was measured using Dual-Luciferase® Reporter Assay System (Promega, Cat# E1960) according to the manufacturer's instructions and the reading were recorded in the GloMax® Multi+ system (Promega).

RNA immunoprecipitation

HEK293T cells were lysed using ice-cold lysis buffer supplemented with 1X protease inhibitor cocktail (11836145001, Roche). The lysate was incubated with FLAG M2 affinity beads overnight at 4°C. The lysate was washed with washing buffer (300 mM NaCl, 50 mM tris-glycine (pH 7.5), 5 mM MgCl2, and 0.05% NP-40). The RNA was extracted using TRIZOL reagent.

Biotin Pull Down Assay

A549 cells were transfected with empty vector and circEPSTI1 plasmid. The cells were lysed post 24 hours after transfection and was incubated with control and circEPSTI1 biotin probe overnight at 4°C. The lysate was incubated with Pierce™ Streptavidin Magnetic Beads (88817, ThermoFisher Scientific) at 4°C for 2 hours. The beads were then washed thrice with lysis buffer and the RNA was extracted using TRIZOL.

Enzyme-linked immunosorbent assay

Culture supernatants from A549 cell lines and PBMC were collected and analyzed by Enzyme-linked immunosorbent assay following the manufacturer's protocols to determine the levels of IP-10 (550926, BD OptEIA™ Human IP-10 ELISA Set) and IL-6 (555220, BD OptEIA™ Human IL-6 ELISA Set).

Immunoblotting analysis

Cells were harvested 36 hours post infection, washed with PBS and lysed with ice-cold lysis buffer containing 1x protease inhibitor cocktail (11836145001, Roche) and 1mM of sodium orthovanadate (S6508, Sigma-Aldrich). The lysate was centrifuged at 15000g for 10 minutes at 4°C and the supernatant was collected. Protein was quantified by Bradford assay and around 10 µg of total protein was loaded. Immunoblotting was done using anti-AKT1 (9Q7, Invitrogen), anti-phospho-Akt (9271, Ser473, Cell Signaling Technology) anti-NS5 (MA5-17295, Invitrogen), anti-NS1 (SAB2700022, Sigma-Aldrich), anti-β actin (A1978, Sigma-Aldrich) antibody. Secondary anti-mouse IgG and anti-rabbit IgG antibodies were purchased from LI-COR. The immunoblotted PVDF membrane was visualized with LI-COR system.

Confocal microscopy

A549 cells were grown under cover slips in 12 well plate. The cells were fixed with acetone: methanol in 1:1 ratio for 10 mins at -20°C. The fixed cells were blocked with BSA supplemented with 0.1% Triton X-100 for permeabilization for 2 hours at room temperature and incubated with primary antibody for 1 hour. The cells were washed three times with PBST and incubated with secondary antibody for 30 minutes at room temperature. The cells were washed three times with PBST, the nucleus was stained with DAPI, and the coverslip was mounted on a glass slide. The cells were then analyzed with LSM 780 confocal laser microscope. ImageJ software was used to analyse the images.

Flow cytometry

Cells were harvested post 36 hours of infection, trypsinized and fixed with 4% formaldehyde for 5 minutes. The cells were permeabilized with 0.1% Triton X-100 for 10 minutes, blocked by 5% FBS for 40 minutes, incubated with primary antibodies for 40 minutes and secondary antibody for 30 minutes. The cells were analyzed using flow cytometer FACSAria III (Becton Dickinson) and the data was analyzed using FlowJo software.

Statistical analysis

All experiments were conducted with appropriate control or mock-transfected samples. Each experiment was repeated independently two or three times. Data were analyzed for statistical significance using GraphPad Prism software. Differences between two groups were assessed using an unpaired, two-tailed Student’s t-test, while differences between three or more groups were evaluated using ANOVA followed by the Newman-Keuls test. Differences were regarded

as statistically significant when $P < 0.05$. Statistical significance in the figures is represented as follows: ***$P < 0.001$, **$P < 0.01$, *$P < 0.05$; ns, not significant.

REFERENCES:

1. J. P. Messina *et al.*, The current and future global distribution and population at risk of dengue. *Nat Microbiol* **4**, 1508-1515 (2019).
2. A. Srikiatkhachorn *et al.*, Dengue--how best to classify it. *Clin Infect Dis* **53**, 563-567 (2011).
3. P. Krishnamoorthy, A. S. Raj, P. Kumar, N. Das, H. Kumar, Host and viral non-coding RNAs in dengue pathogenesis. *Rev Med Virol* **32**, e2360 (2022).
4. H. Kumar, T. Kawai, S. Akira, Toll-like receptors and innate immunity. *Biochem Biophys Res Commun* **388**, 621-625 (2009).
5. J. Sprokholt, L. C. Helgers, T. B. Geijtenbeek, Innate immune receptors drive dengue virus immune activation and disease. *Future Virol* **13**, 287-305 (2017).
6. Y. T. Kao, M. M. C. Lai, C. Y. Yu, How Dengue Virus Circumvents Innate Immunity. *Front Immunol* **9**, 2860 (2018).
7. Y. Wang *et al.*, Circular RNAs in human diseases. *MedComm (2020)* **5**, e699 (2024).
8. A. Gu *et al.*, Functions of Circular RNA in Human Diseases and Illnesses. *Noncoding RNA* **9** (2023).
9. H. Ingle *et al.*, The microRNA miR-485 targets host and influenza virus transcripts to regulate antiviral immunity and restrict viral replication. *Sci Signal* **8**, ra126 (2015).
10. T. Tagawa *et al.*, Discovery of Kaposi's sarcoma herpesvirus-encoded circular RNAs and a human antiviral circular RNA. *Proc Natl Acad Sci U S A* **115**, 12805-12810 (2018).
11. A. D. Pandey *et al.*, Correlation of altered expression of a long non-coding RNA, NEAT1, in peripheral blood mononuclear cells with dengue disease progression. *J Infect* **75**, 541-554 (2017).
12. A. Kumar *et al.*, MicroRNA hsa-miR-324-5p Suppresses H5N1 Virus Replication by Targeting the Viral PB1 and Host CUEDC2. *J Virol* **92** (2018).
13. A. Quillet *et al.*, Improving Bioinformatics Prediction of microRNA Targets by Ranks Aggregation. *Front Genet* **10**, 1330 (2019).
14. N. Diehl, H. Schaal, Make yourself at home: viral hijacking of the PI3K/Akt signaling pathway. *Viruses* **5**, 3192-3212 (2013).
15. J. He *et al.*, hsa_circ_0006459 and hsa_circ_0015962 affect prognosis of Dengue fever. *Sci Rep* **9**, 19425 (2019).
16. P. Wu *et al.*, circEPSTI1 promotes tumor progression and cisplatin resistance via upregulating MSH2 in cervical cancer. *Aging (Albany NY)* **14**, 5406-5416 (2022).
17. P. Wu *et al.*, Circular RNA circEPSTI1 accelerates cervical cancer progression via miR-375/409-3P/515-5p-SLC7A11 axis. *Aging (Albany NY)* **13**, 4663-4673 (2021).
18. X. Tan *et al.*, circEPSTI1 Acts as a ceRNA to Regulate the Progression of Osteosarcoma. *Curr Cancer Drug Targets* **20**, 288-294 (2020).
19. B. Chen *et al.*, circEPSTI1 as a Prognostic Marker and Mediator of Triple-Negative Breast Cancer Progression. *Theranostics* **8**, 4003-4015 (2018).
20. Y. Xie, L. Wang, D. Yang, CircEPSTI1 Promotes the Progression of Non-Small Cell Lung Cancer Through miR-145/HMGB3 Axis. *Cancer Manag Res* **12**, 6827-6836 (2020).
21. T. Yang *et al.*, Downregulation of circEPSTI1 represses the proliferation and invasion of non-small cell lung cancer by inhibiting TRIM24 via miR-1248 upregulation. *Biochem Biophys Res Commun* **530**, 348-354 (2020).
22. J. Xie *et al.*, circEPSTI1 regulates ovarian cancer progression via decoying miR-942. *J Cell Mol Med* **23**, 3597-3602 (2019).
23. J. Wang *et al.*, The circEPSTI1/mir-942-5p/LTBP2 axis regulates the progression of OSCC in the background of OSF via EMT and the PI3K/Akt/mTOR pathway. *Cell Death Dis* **11**, 682 (2020).

24. Z. Cui *et al.*, The Combination of circEPSTI1 and MIF Offers Diagnostic Value for Endometrial Cancer. *Int J Gen Med* **17**, 1395-1403 (2024).
25. X. Wang *et al.*, CircEPSTI1 in peripheral blood as a novel potential biomarker for childhood-onset systemic lupus erythematosus. *Rheumatology & Autoimmunity* **4**, 20-26 (2024).
26. T. Kawai, S. Akira, Toll-like receptor and RIG-I-like receptor signaling. *Ann N Y Acad Sci* **1143**, 1-20 (2008).
27. Z. Liang *et al.*, Activation of Toll-like receptor 3 impairs the dengue virus serotype 2 replication through induction of IFN-beta in cultured hepatoma cells. *PLoS One* **6**, e23346 (2011).
28. J. P. Wang *et al.*, Flavivirus activation of plasmacytoid dendritic cells delineates key elements of TLR7 signaling beyond endosomal recognition. *J Immunol* **177**, 7114-7121 (2006).
29. J. K. Sprokholt *et al.*, RIG-I-like Receptor Triggering by Dengue Virus Drives Dendritic Cell Immune Activation and T(H)1 Differentiation. *J Immunol* **198**, 4764-4771 (2017).
30. D. Yang *et al.*, MiR-942 mediates hepatitis C virus-induced apoptosis via regulation of ISG12a. *PLoS One* **9**, e94501 (2014).
31. P. Karyala *et al.*, DenHunt - A Comprehensive Database of the Intricate Network of Dengue-Human Interactions. *PLoS Negl Trop Dis* **10**, e0004965 (2016).
32. V. S. Lekshmi *et al.*, PI3K/Akt/Nrf2 mediated cellular signaling and virus-host interactions: latest updates on the potential therapeutic management of SARS-CoV-2 infection. *Front Mol Biosci* **10**, 1158133 (2023).
33. A. Lahon, R. P. Arya, A. C. Banerjea, Dengue Virus Dysregulates Master Transcription Factors and PI3K/AKT/mTOR Signaling Pathway in Megakaryocytes. *Front Cell Infect Microbiol* **11**, 715208 (2021).
34. A. Banerjee *et al.*, RNA-Seq analysis of peripheral blood mononuclear cells reveals unique transcriptional signatures associated with disease progression in dengue patients. *Transl Res* **186**, 62-78 e69 (2017).
35. S. Chen, Y. Zhou, Y. Chen, J. Gu, fastp: an ultra-fast all-in-one FASTQ preprocessor. *Bioinformatics* **34**, i884-i890 (2018).
36. H. Li, R. Durbin, Fast and accurate short read alignment with Burrows-Wheeler transform. *Bioinformatics* **25**, 1754-1760 (2009).
37. Y. Gao, J. Zhang, F. Zhao, Circular RNA identification based on multiple seed matching. *Brief Bioinform* **19**, 803-810 (2018).
38. J. Zhang, S. Chen, J. Yang, F. Zhao, Accurate quantification of circular RNAs identifies extensive circular isoform switching events. *Nat Commun* **11**, 90 (2020).
39. M. I. Love, W. Huber, S. Anders, Moderated estimation of fold change and dispersion for RNA-seq data with DESeq2. *Genome Biol* **15**, 550 (2014).
40. A. D. Davidson, Development and application of dengue virus reverse genetic systems. *Methods Mol Biol* **1138**, 113-130 (2014).

Acknowledgement:

This work was supported by the intramural research grant from the Indian Institute of Science Education and Research, Bhopal (IISER Bhopal). The funders had no role in study design, data collection, interpretation, or the decision to submit the work for publication. The pIRESneo-Flag/HA Ago2 plasmid was a gift from T. Tuschl (Addgene; plasmid 10822). The DENV-2 reverse genetics system was a kind gift from Prof. Davidson. We thank IISER Bhopal for providing access to the Central Instrumentation Facility.

Contributions:

Nilanjana Das – Conceptualization, Methodology, Validation, Formal Analysis, Investigation, Data curation, Writing – Original Draft, Writing- Review & Editing, Visualization.

Pandikannan Krishnamoorthy - Conceptualization, Methodology, Software, Formal Analysis, Investigation, Data curation, Writing – Original Draft, Writing- Review & Editing, Visualization.

Kushal Ramrao Junghare- Investigation, Validation, Visualization, Writing- Review & Editing.

Athira S Raj- Investigation, Visualization, Data curation, Writing- Review & Editing.

Priyanka De- Resources, Writing- Review & Editing

Shouvanik Adhya - Resources, Writing- Review & Editing

Atul Garg – Resources, Writing- Review & Editing

Dheeraj Kheten – Resources, Writing- Review & Editing

Ashok Kumar- Resources, Writing- Review & Editing

Himanshu Kumar- Conceptualization, Methodology, Formal Analysis, Data curation, Writing – Original Draft, Writing- Review & Editing, Project administration, Funding Acquisition Visualization, Supervision

Ethics declarations

Experiments were performed after approval from the Institutional Ethical Committee (IEC), Indian Institute of Science Education and Research (IISER) Bhopal (IISERB/IEC/Certificate/20l7-II/01). The Dengue patient samples were obtained from the College of Medicine and JNM Hospital, Kalyani, West Bengal. The IEC approval number for the patient samples is F-24/PR/COMJNMH/IEC/24/2/42.

Declaration of interests

The authors declare no competing interests.

Figure Legends

Figure 1:

Computational analysis of DENV-clinical samples identifies the upregulation of circEPSTI1

(A) Distribution of sequencing reads mapped to the human genome: mapped reads (blue), unmapped reads (green), both in millions, and circular reads (orange), in thousands across samples from dataset GSE94892, supporting high-depth circRNA profiling in DENV-infected human PBMCs. (B) Volcano plot showing differentially expressed circRNAs between control and DENV-infected groups. Red points indicate statistically significant circRNAs based on log fold change and adjusted p-values. The top three circRNAs are annotated with arrows. (C) Dot plot depicting normalized expression levels of the top five circRNAs. The red dotted line is the threshold with the normalized value of 5, above which the circRNAs are expressed at a higher level. (D) Schematic of circEPSTI1 biogenesis from EPSTI1 pre-mRNA and the primer design. circEPSTI1 and EPSTI1 levels were measured from the cDNA synthesized with the random hexamer method, the oligo-dT primers method, and the genomic DNA and cDNA as templates from the PBMCs for the amplification. (E) Sanger sequencing of the amplified bands using specific divergent primers spanning the back-splice junction. (F) Pre-treatment of Actinomycin D (10µg/ml) was performed for the indicated times, and the expression of linear EPSTI1 and circEPSTI1 was measured. (G) DENV (48hr) infected cellular RNA from PBMCs was treated with and without RNase R (2U/µl), and linear EPSTI1 and circEPSTI1 were quantified by qPCR. (H) DENV (48hr) infected cellular RNA from PBMCs isolated from cytoplasmic and nuclear cell fractionation was used to quantify circEPSTI1 by qPCR (I) Confocal microscopy images of A549 cells using cy3-labeled probes targeting circEPSTI1 for localization of

circEPSTI1. Data are mean ± SEMs from triplicate samples of a single experiment and are representative of results from three independent experiments.

Figure 2:

DENV infection induced circEPSTI1 depends on the RLR pathway, in vitro and ex vivo.

(A) Schematic of clinical recruitment of DENV patients' plasma from India, and circEPSTI1 levels were measured using qPCR in healthy controls and DENV patients. (B) Human PBMCs (PBMC) of healthy volunteers were infected with DENV (MOI=1) for 36h ex vivo, and circEPSTI1 levels were measured in cells using qPCR. (C) The copy number of circEPSTI1 was measured using digital-PCR in the DENV-infected (MOI=0.5) and mock-infected A549 cells at 36h. (D) Different cell lines, such as A549 (Lung), MRC5 (Lung) (MOI=0.5), and HepG2 (Liver) (MOI=0.5), and primary cells, PBMCs, were infected with DENV and the circEPSTI1 level was measured at 12, 24, 36, and 48h post-infection. A549 cells were treated with Poly I:C. (E), recombinant IFN-α (F), and recombinant IFN-β (G), and the level of circEPSTI1 was measured at 6, 12, and 18h. (H) DENV infection (MOI=0.5) was performed in wild-type (WT), RIG-I (Sensor) Knock-out (KO), IPS-1 (Adaptor) KO, or IRF-3 (transcription factor) KO A549 cells at 12, 24, 36, and 48 h, and the expression of circEPSTI1 was measured. (I) Mock and DENV-2 infected A549 cells were fixed and hybridized with cy3-labelled circEPSTI1 probe and subjected to confocal microscopy. Data are mean ± SEMs from triplicate samples of a single experiment and are representative of results from three independent experiments. ****, $p < 0.0001$, ***$p < 0.001$ **, $p < 0.01$, and *$p < 0.05$, by two-tailed unpaired t test (B). ns, nonsignificant.

Figure 3:

DENV establishes infection through circEPSTI1

(A) siRNA-mediated knockdown of circEPSTI1 was performed by designing the siRNA against the back-splice junction as shown in the schematic. PBMC and A549 cells were transfected with circEPSTI1 siRNA for 24h, and subsequently, the cells were infected with DENV (MOI=0.5) for 36h. Knockdown efficiency was tested by qPCR. (B) Intracellular viral load was measured by qPCR. (C) Viral load in the culture supernatant was measured upon circEPSTI1 knockdown by qPCR. A549 cells transfected with circEPSTI1 siRNA were infected with DENV (MOI=0.5) for 36h. DENV viral load at protein level (NS5) upon circEPSTI1 knockdown was quantified using the (D) western blot, (E) FACS analysis, and (F) confocal microscopy using DENV NS5-specific antibody. Nuclei were stained with DAPI. (G) circEPSTI1 was cloned in Circminivector mneon v2 vector, as shown in the schematic. A549 cells were transfected with the overexpression vector and infected with DENV (MOI=0.5) for 36h, and overexpression was tested by q-PCR. A549 cells transfected with the circEPSTI1 vector were infected with DENV (MOI=0.5) for 36h. Viral load in cells (H) and culture supernatant (I) and was tested by qPCR. DENV NS5 protein level in circEPSTI1 was quantified through western blot analysis. (J) FACS analysis and confocal microscopy (L) using DENV NS5 antibody. Nuclei were stained with DAPI. IFNβ and OAS2 levels were tested by qPCR upon (M) circEPSTI1 knockdown and (N) circEPSTI1 overexpressed A549 cells. The levels of interferon induced protein IP-10 and inflammatory cytokine IL-6 were quantified using ELISA upon (O) circEPSTI1 knockdown and (P) circEPSTI1 overexpression. Data are mean ± SEMs from triplicate samples of a single experiment and are representative of results from three independent experiments. ****, $p <$

0.0001, ∗∗∗, $p < 0.001$, ∗∗, $p < 0.01$, and ∗, $p < 0.05$, by two-tailed unpaired t test (B). ns, nonsignificant.

Figure 4:

CircEPSTI1 sponges hsa-miR-942-5p

(A) Three RNA interaction prediction algorithms, miRanda, PITA, and TargetScan, were employed to predict the interaction of miRNAs with circEPSTI1 with a stringent cutoff: miRanda - Binding energy cutoff -40 kcal/mol and minimum miRanda Score of 300; PITA - PITA score of minimum -10 and number of binding sites to be minimum 6; TargetScan - more than one binding site. (B & C) circEPSTI1 wild type (WT) and mutant (M) sequences were cloned downstream of luciferase HEK293T cells were transfected with indicated, 100ng of circEPSTI1-luc (WT) or mut circEPSTI1 (M), 25nM miR-942-5p mimic or 25nM miR-942-5p inhibitor, and 30ng pRL-TK vector. Luciferase assay was performed after 48h. (D) HEK293T cells were transfected with 2µg of plasmid encoding Flag-Ago2 and 25nM mir-942 and were infected with DENV virus (MOI=2) for 36h. RNA immunoprecipitation was done using FLAG-M2 beads, and the enrichment of miR-942 was tested by qPCR. (E) A biotin-labeled circEPSTI1 probe was used to pull down the RNA fractions binding to the circEPSTI1, and the level of miR-942 was measured by qPCR. (F) Upon knockdown of circEPSTI1, miR-942-5p expression was quantified in PBMC and A549 cells by qPCR. (G) A549 cells were transfected with sicirEPSTI1 and sicircEPSTI1 along with miR-942 inhibitor. miR-942 level and viral load were quantified by qPCR. (H) miR-942-5p levels upon DENV infection at different time points were quantified in PBMC (MOI =1), A549 (MOI=0.5), MRC5(MOI=0.5), and HEPG2(MOI=0.5) by qPCR. Data are mean ± SEMs from triplicate samples of a single experiment and are representative of results

from three independent experiments. ****, $p < 0.0001$, ***$p < 0.001$ **, $p < 0.01$, and *$p < 0.05$, by two-tailed unpaired t test (B). ns, nonsignificant.

Figure 5:

miR-942-5p targets DENV genomic RNA and suppresses viral replication

(A) Predicted binding sites of miR-942-5p across the genomes of four different DENV serotypes. (B) NS1, NS5, NS3, and NS2B sequences were cloned downstream of the pmiR-luciferase vector. HEK293T cells were transfected with 100ng of NS1, NS3, NS5, and NS2B luciferase constructs, 25nM of miR-942 mimic, and 30ng of PRL-Tk plasmid. Luciferase assay was performed after 48h. (C) A549 cells were transfected with 2µg of FLAG-Ago2 plasmid and 50 nM of miR-942 mimic, followed by DENV infection for 36h. RNA immunoprecipitation was done using FLAG-M2 beads, and the enrichment of virus was tested by qPCR. (D) A549 cells and PBMCs were transfected with 25nM of miR-942 mimic and 25nM of miR-942 inhibitor for 24h and infected with DENV for 36h. The viral load was quantified by qPCR. (E) Viral load in the supernatant of A549 cells was quantified by qPCR. (F) DENV NS1 and NS5 protein level in miR-942 overexpressed A549 cells was quantified through western blot analysis. (G) FACS analysis was performed with the DENV NS5-specific antibody upon miR-942 overexpression in A549 cells. (H) A549 cells transfected with miR-942 mimic were infected with DENV for 36h and were subjected to confocal microscopy using DENV NS1 and NS5 antibody. Nuclei were stained with DAPI. (I) The levels of interferon induced protein IP-10 and inflammatory cytokine IL-6 were quantified using ELISA upon miR-942 overexpression in A549 cells. A549 cells and PBMCs were infected with DENV at an MOI=0.5 and MOI=1 respectively. Data are mean ± SEMs from triplicate samples of a single experiment and are representative of results from three

independent experiments. ****, $p < 0.0001$, ***$p < 0.001$ **, $p < 0.01$, and *$p < 0.05$, by two-tailed unpaired t test (B). ns, nonsignificant.

Figure 6:

circ-ESPTI1-regulated miR-942-5p affects host AKT-signaling upon DENV infection

(A) The host targets of miR-942-5p were tested using miRabeL. (B) The expression of AKT1 and p-AKT1 at the protein level was quantified using western blot analysis at 6, 12, 24, 36, and 48h in DENV-infected A549 cells. (C) AKT1-3' UTR sequence was cloned downstream of the pmiR-luciferase vector. HEK293T cells were transfected with 100ng of AKT1-3'UTR luciferase construct, 25nM of miR-942 mimic, 25nM of miR-942 inhibitor and 30ng of PRL-Tk plasmid. Luciferase assay was performed after 48h. (D) HEK293T cells were transfected with 100ng of WT AKT1-luc, 100ng of Mut AKT1-luc, 25nM miR-942-5p mimic, and 30ng pRL-TK vector. Luciferase assay was performed after 48h. (E) A549 cells were transfected with 2µg of FLAG-Ago2 plasmid and 50 nM of miR-942 mimic, followed by DENV infection for 36h. RNA immunoprecipitation was done using FLAG-M2 beads and the enrichment of AKT1 was tested by qPCR. (F) A549 cells were transfected with 25nM of miR-942 mimic for 24h and infected with DENV for 36h. DENV NS5 and AKT1 protein level was quantified through western blot analysis. (G) A549 cells were transfected with 25nM of AKT1 siRNA for 24h and infected with DENV for 36h. Efficiency knockdown of AKT1 and viral load was quantified by qPCR. (H) DENV NS5 protein level in siAKT1 transfected A549 cells was quantified through western blot analysis (I) FACS analysis was performed with the DENV NS5 specific antibody upon knockdown of AKT1 in A549 cells. (J) A549 cells transfected with siAKT1 was infected with DENV for 36h and was subjected to confocal microscopy using DENV NS5 antibody. Nuclei

were stained with DAPI. (K) IFNβ and OAS2 levels were checked by qPCR upon AKT1 knockdown. An increased dose of siRNA targeting circEPSTI1 reduced AKT1 level, in turn, led to the proviral activity of circEPSTI1. (L) The levels of interferon induced protein IP-10 and inflammatory cytokine IL-6 were quantified using ELISA upon AKT1 knockdown (M) A549 cells were transfected with increased doses of sicircEPSTI1 for 24h and infected with DENV for 36h. AKT1 protein level was quantified through western blot analysis. (N) A549 cells were infected with DENV and treated with 20uM and 40uM of Wortmannin (WM), an AKT1 pharmacological inhibitor for 36h. pAKT1 and DENV NS5 protein level was quantified through western blot analysis. (O) A549 cells were infected with DENV and treated with 20uM WM for 36h and was subjected to confocal microscopy using DENV NS5 antibody. Nuclei were stained with DAPI. A549 cells were infected with DENV at an MOI=0.5.

Data are mean ± SEMs from triplicate samples of a single experiment and are representative of results from three independent experiments. ****, $p < 0.0001$, ***, $p < 0.001$, **, $p < 0.01$, and *, $p < 0.05$, by two-tailed unpaired t test (B). ns, nonsignificant.

Fig 1.

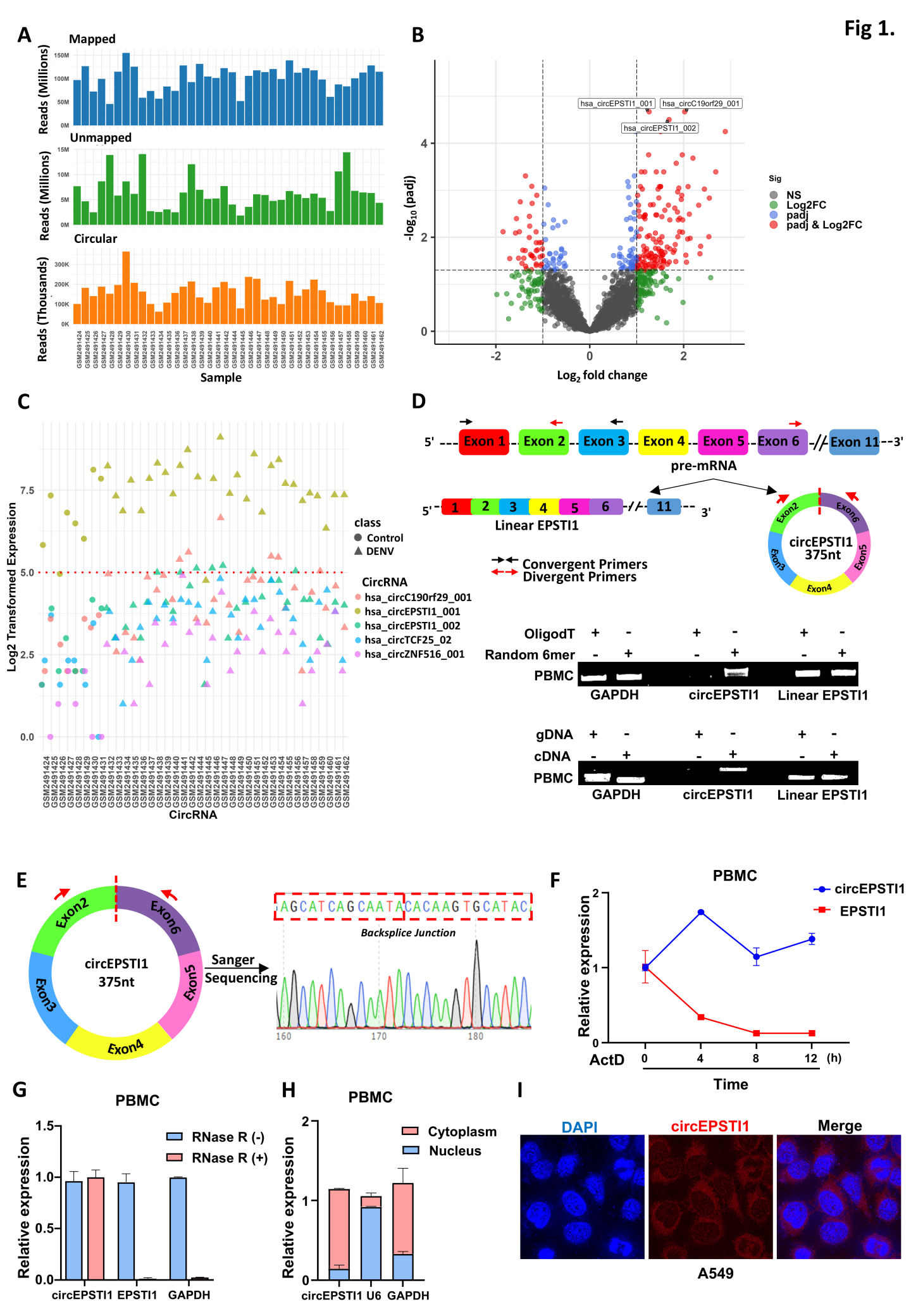
A
Mapped
Reads (Millions)
Unmapped
Reads (Millions)
Circular
Reads (Thousands)
Sample
B
hsa_circEPSTI1_001
hsa_circC19orf29_001
hsa_circEPSTI1_002
-log10 (padj)
Log2 fold change
Sig
NS
Log2FC
padj
padj & Log2FC
C
Log2 Transformed Expression
class
Control
DENV
CircRNA
hsa_circC190rf29_001
hsa_circEPSTI1_001
hsa_circEPSTI1_002
hsa_circTCF25_02
hsa_circZNF516_001
CircRNA
D
5'
Exon 1
Exon 2
Exon 3
Exon 4
Exon 5
Exon 6
Exon 11
3'
pre-mRNA
Linear EPSTI1
circEPSTI1
375nt
Convergent Primers
Divergent Primers
OligodT
Random 6mer
PBMC
GAPDH
circEPSTI1
Linear EPSTI1
gDNA
cDNA
E
circEPSTI1
375nt
Exon2
Exon6
Exon5
Exon4
Exon3
Sanger
Sequencing
Backsplice Junction
F
PBMC
circEPSTI1
EPSTI1
Relative expression
ActD
Time
(h)
G
PBMC
RNase R (-)
RNase R (+)
Relative expression
circEPSTI1
EPSTI1
GAPDH
H
PBMC
Cytoplasm
Nucleus
Relative expression
circEPSTI1
U6
GAPDH
I
DAPI
circEPSTI1
Merge
A549

Fig 2.

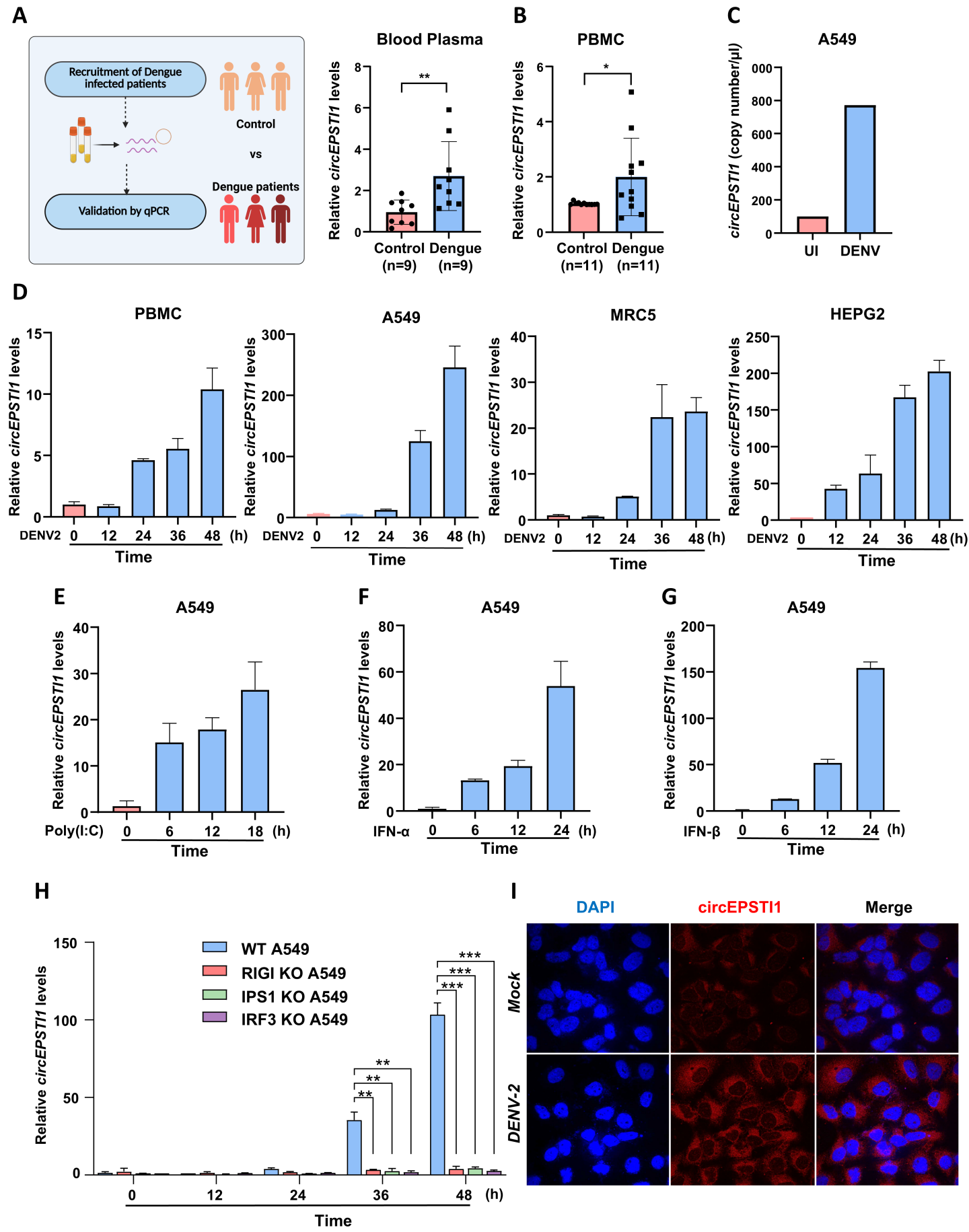
A
Recruitment of Dengue infected patients
Control
vs
Dengue patients
Validation by qPCR
Blood Plasma
Relative circEPSTI1 levels
Control (n=9)
Dengue (n=9)
B
PBMC
Control (n=11)
Dengue (n=11)
C
A549
circEPSTI1 (copy number/μl)
UI
DENV
D
PBMC
A549
MRC5
HEPG2
DENV2
Time
E
A549
Poly(I:C)
F
A549
IFN-α
G
A549
IFN-β
H
WT A549
RIGI KO A549
IPS1 KO A549
IRF3 KO A549
I
DAPI
circEPSTI1
Merge
Mock
DENV-2

Fig 3.

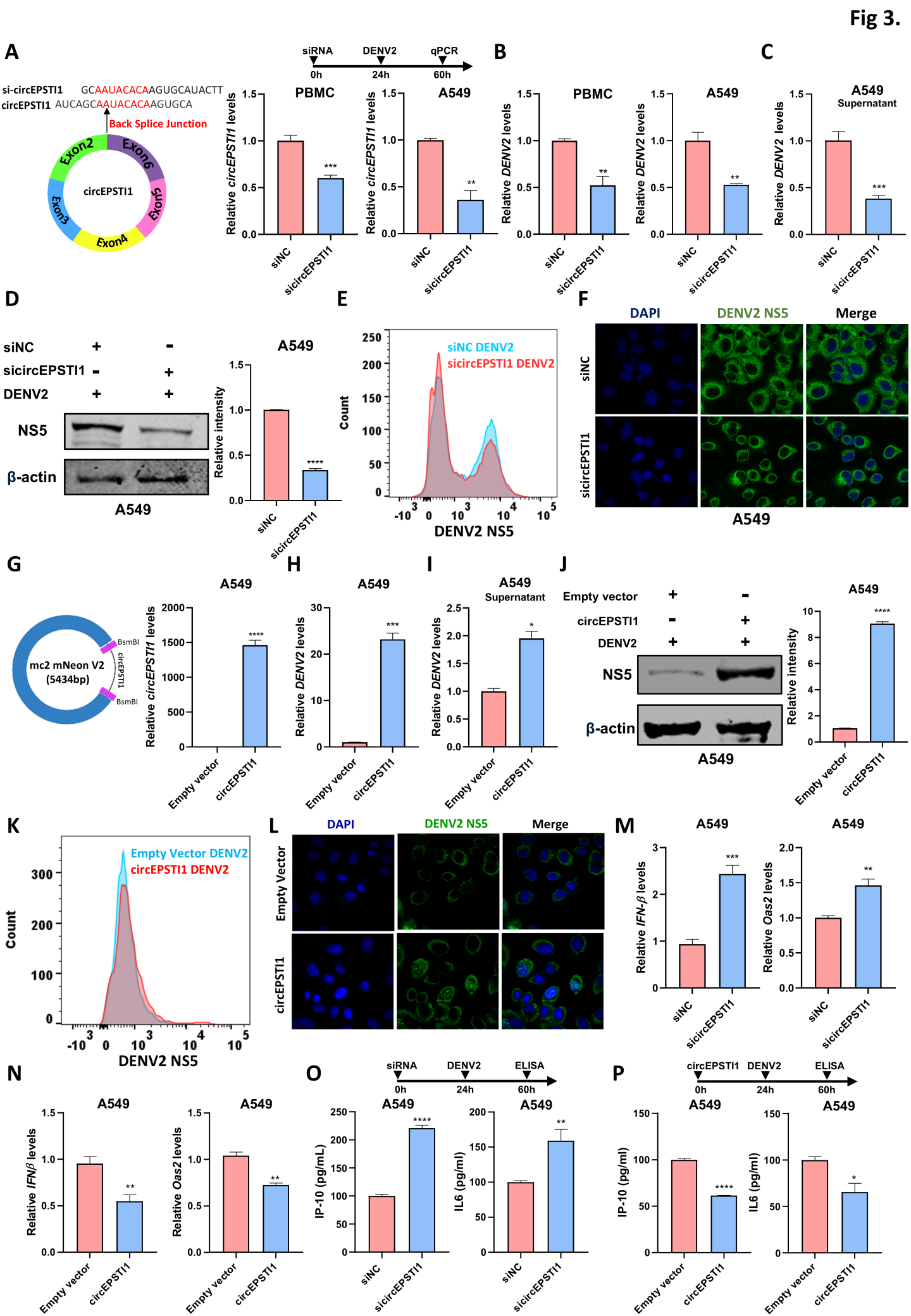
A
si-circEPSTI1 GCAAUACACAAGUGCAUACTT
circEPSTI1 AUCAGCAAUACACAAGUGCA
Back Splice Junction
Exon2
Exon6
Exon5
Exon4
Exon3
circEPSTI1
siRNA
DENV2
qPCR
0h
24h
60h
PBMC
A549
Relative circEPSTI1 levels
siNC
sicircEPSTI1
B
Relative DENV2 levels
C
A549
Supernatant
D
siNC
sicircEPSTI1
DENV2
NS5
β-actin
Relative intensity
E
siNC DENV2
sicircEPSTI1 DENV2
Count
DENV2 NS5
F
DAPI
DENV2 NS5
Merge
G
mc2 mNeon V2
(5434bp)
BsmBI
circEPSTI1
Empty vector
circEPSTI1
H
I
J
K
Empty Vector DENV2
circEPSTI1 DENV2
L
Empty Vector
circEPSTI1
M
Relative IFN-β levels
Relative Oas2 levels
N
O
siRNA
DENV2
ELISA
IP-10 (pg/mL)
IL6 (pg/ml)
P
circEPSTI1
DENV2
ELISA

Fig 4.

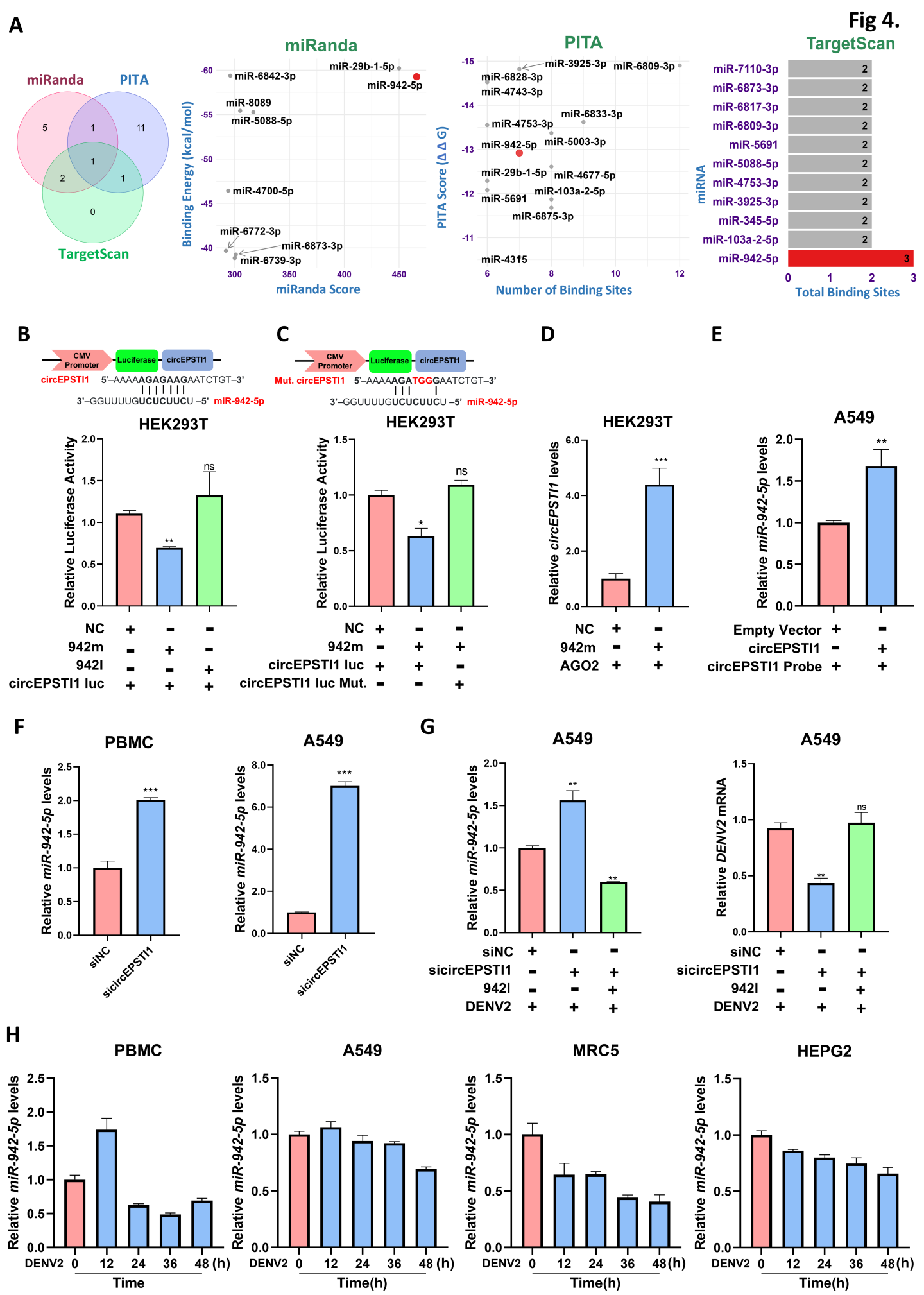
A
miRanda
PITA
TargetScan
5
1
11
1
2
1
0
miRanda
Binding Energy (kcal/mol)
miRanda Score
miR-29b-1-5p
miR-6842-3p
miR-942-5p
miR-8089
miR-5088-5p
miR-4700-5p
miR-6772-3p
miR-6873-3p
miR-6739-3p
PITA
PITA Score (Δ Δ G)
Number of Binding Sites
miR-3925-3p
miR-6809-3p
miR-6828-3p
miR-4743-3p
miR-6833-3p
miR-4753-3p
miR-942-5p
miR-5003-3p
miR-29b-1-5p
miR-4677-5p
miR-103a-2-5p
miR-5691
miR-6875-3p
miR-4315
TargetScan
miRNA
Total Binding Sites
miR-7110-3p
miR-6873-3p
miR-6817-3p
miR-6809-3p
miR-5691
miR-5088-5p
miR-4753-3p
miR-3925-3p
miR-345-5p
miR-103a-2-5p
miR-942-5p
B
CMV Promoter
Luciferase
circEPSTI1
circEPSTI1 5'–AAAAAGAGAAGAATCTGT–3'
3'–GGUUUUGUCUCUUCU –5' miR-942-5p
HEK293T
Relative Luciferase Activity
ns
**
NC
942m
942I
circEPSTI1 luc
C
Mut. circEPSTI1 5'–AAAAAGATGGGAATCTGT–3'
3'–GGUUUUGUCUCUUCU –5' miR-942-5p
HEK293T
Relative Luciferase Activity
ns
*
NC
942m
circEPSTI1 luc
circEPSTI1 luc Mut.
D
HEK293T
Relative circEPSTI1 levels
***
NC
942m
AGO2
E
A549
Relative miR-942-5p levels
**
Empty Vector
circEPSTI1
circEPSTI1 Probe
F
PBMC
Relative miR-942-5p levels
***
siNC
sicircEPSTI1
A549
Relative miR-942-5p levels
***
siNC
sicircEPSTI1
G
A549
Relative miR-942-5p levels
**
**
siNC
sicircEPSTI1
942I
DENV2
A549
Relative DENV2 mRNA
ns
**
siNC
sicircEPSTI1
942I
DENV2
H
PBMC
A549
MRC5
HEPG2
Relative miR-942-5p levels
DENV2 0 12 24 36 48 (h)
Time
Time(h)

Fig 5.

A

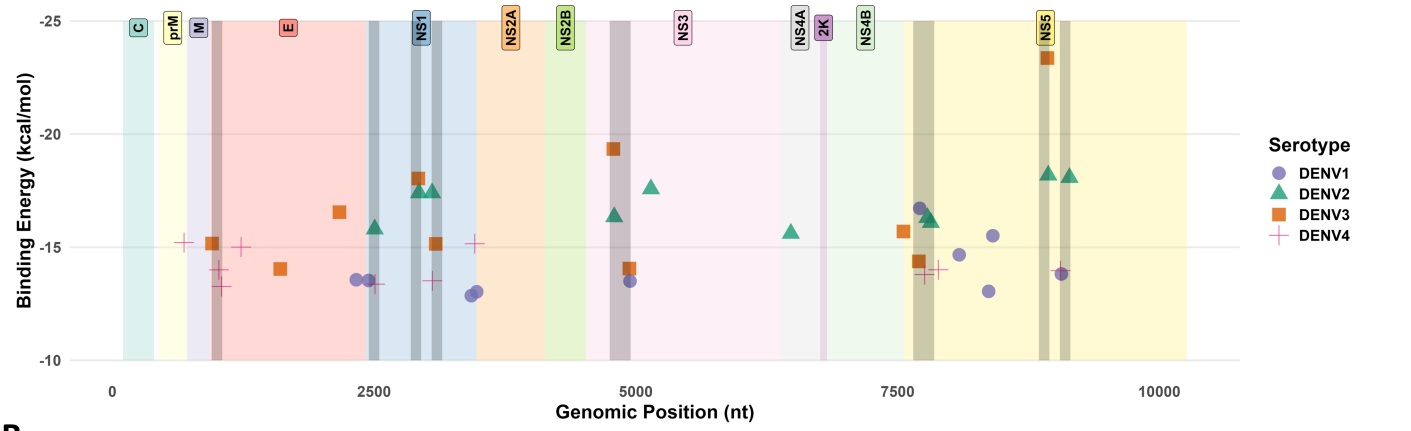

B

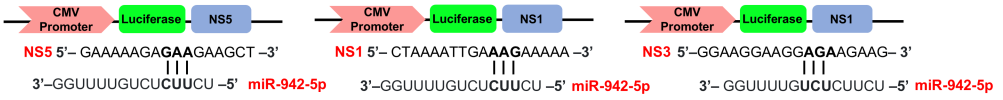

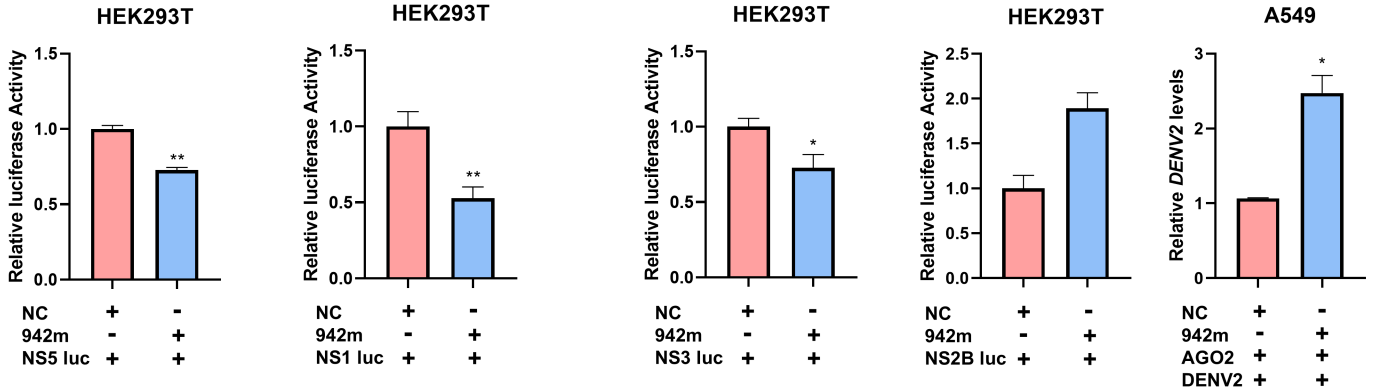

C

D

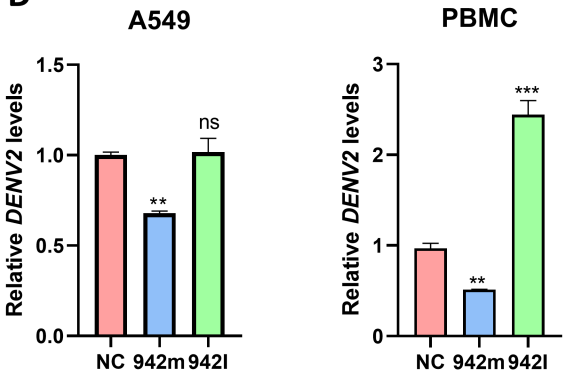

E

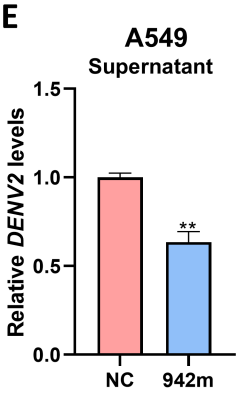

F

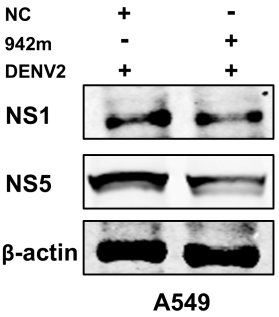

G

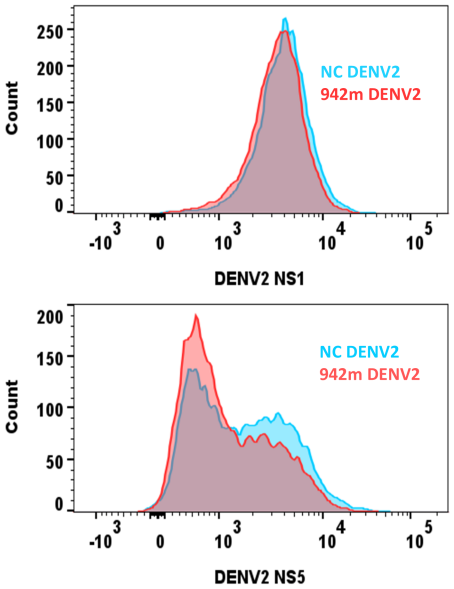

H

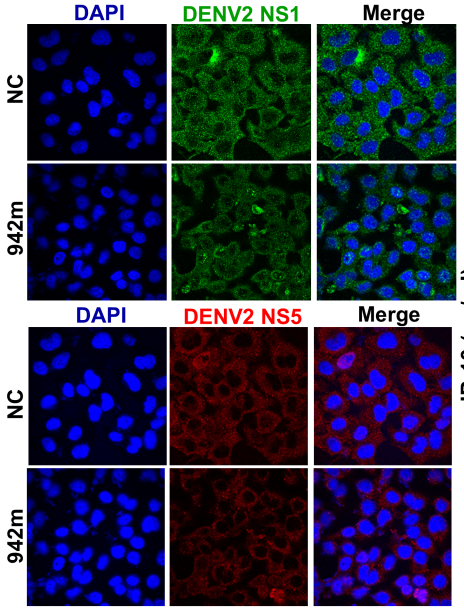

I

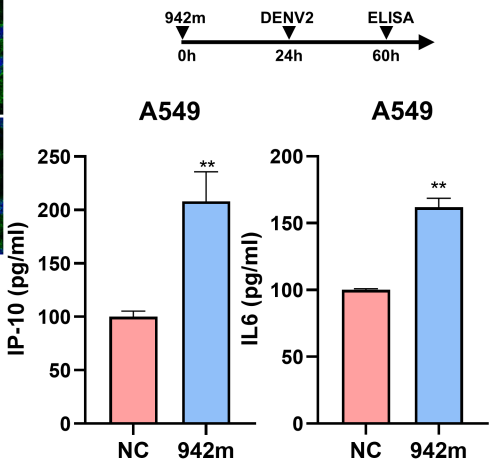

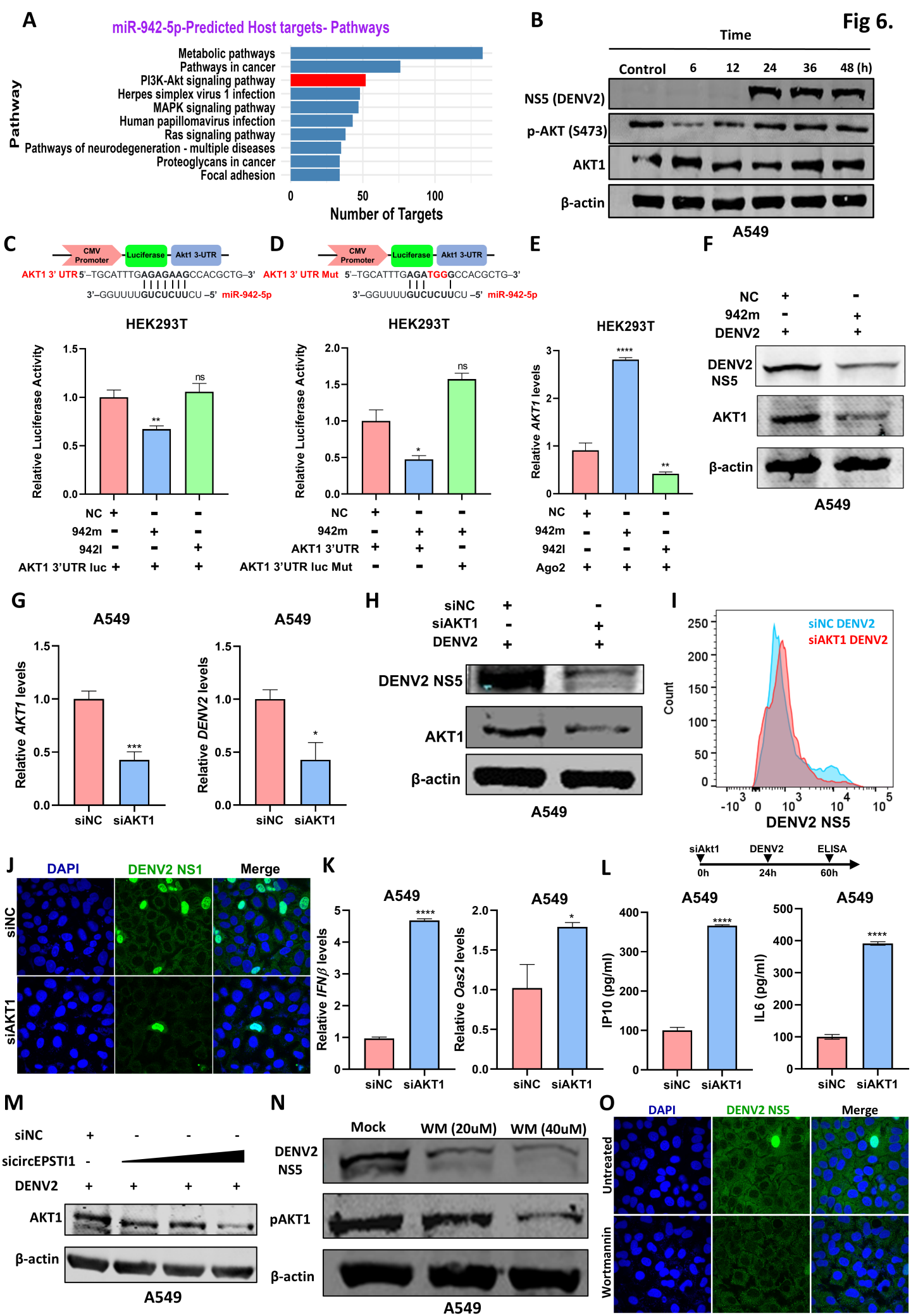
Fig 6.
A
miR-942-5p-Predicted Host targets- Pathways
Pathway
Metabolic pathways
Pathways in cancer
PI3K-Akt signaling pathway
Herpes simplex virus 1 infection
MAPK signaling pathway
Human papillomavirus infection
Ras signaling pathway
Pathways of neurodegeneration - multiple diseases
Proteoglycans in cancer
Focal adhesion
0
50
100
Number of Targets
B
Time
Control
6
12
24
36
48 (h)
NS5 (DENV2)
p-AKT (S473)
AKT1
β-actin
A549
C
CMV Promoter
Luciferase
Akt1 3-UTR
AKT1 3' UTR 5'–TGCATTTGAGAGAAGCCACGCTG–3'
3'–GGUUUUGUCUCUUCU –5' miR-942-5p
HEK293T
Relative Luciferase Activity
NC
942m
942l
AKT1 3'UTR luc
D
AKT1 3' UTR Mut 5'–TGCATTTGAGATGGGCCACGCTG–3'
3'–GGUUUUGUCUCUUCU –5' miR-942-5p
AKT1 3'UTR
AKT1 3'UTR luc Mut
E
Relative AKT1 levels
Ago2
F
DENV2
DENV2 NS5
AKT1
β-actin
A549
G
A549
Relative AKT1 levels
Relative DENV2 levels
siNC
siAKT1
H
siNC
siAKT1
DENV2
DENV2 NS5
AKT1
β-actin
A549
I
siNC DENV2
siAKT1 DENV2
Count
DENV2 NS5
J
DAPI
DENV2 NS1
Merge
siNC
siAKT1
K
A549
Relative IFNβ levels
Relative Oas2 levels
siNC
siAKT1
L
siAkt1
DENV2
ELISA
0h
24h
60h
IP10 (pg/ml)
IL6 (pg/ml)
M
siNC
sicircEPSTI1
DENV2
AKT1
β-actin
A549
N
Mock
WM (20uM)
WM (40uM)
DENV2 NS5
pAKT1
β-actin
A549
O
DAPI
DENV2 NS5
Merge
Untreated
Wortmannin